iEnergy
ARTICLE
https://doi.org/10.23919/IEN.2024.0001

25% – Efficiency flexible perovskite solar cells via controllable growth of SnO_2

Ningyu Ren[1,†], Liguo Tan[1,†], Minghao Li[1,†], Junjie Zhou[1], Yiran Ye[1], Boxin Jiao[1], Liming Ding[2] and Chenyi Yi[1] ✉

ABSTRACT

High power conversion efficiency (PCE) flexible perovskite solar cells (FPSCs) are highly desired power sources for aerospace crafts and flexible electronics. However, their PCEs still lag far behind their rigid counterparts. Herein, we report a high PCE FPSC by controllable growth of a SnO_2 electron transport layer through constant pH chemical bath deposition (CBD). The application of $SnSO_4$ as tin source enables us to perform CBD without strong acid, which in turn makes it applicable to acid-sensitive flexible indium tin oxide. Furthermore, a mild and controllable growth environment leads to uniform particle growth and dense SnO_2 deposition with full coverage and reproducibility, resulting in a record PCE of up to 25.09% (certified 24.90%) for FPSCs to date. The as-fabricated FPSCs exhibited high durability, maintaining over 90% of their initial PCE after 10000 bending cycles.

KEYWORDS

Flexible perovskite solar cells, chemical bath deposition, SnO_2, electron transport layer.

Flexible perovskite solar cells (FPSCs) have attracted great attention because of their unique advantages in lightweight and portable electronics applications[1–9]. The champion power conversion efficiency (PCE) increased dramatically from 2.6% in 2013 to 24.0% in 2023[10–12], outperforming other flexible solar cell counterparts and showing a promising future in the abundant application scenario. However, the efficiency of FPSCs is significantly lower than that of rigid devices, which has surpassed 26%[13]. Due to the soft and inhomogeneous nature of the flexible PET substrate utilized in FPSCs, coating perovskite films onto large-area flexible substrates poses significant challenges. Additionally, the low glass transition temperature of PET material renders it susceptible to curling during the perovskite preparation process. Unlike rigid PSCs, which utilize glass substrates, flexible substrates possess pores that act as potential invasion sites for water and oxygen, leading to the undesirable decomposition of perovskite materials[14]. Effective measures need to be implemented to further improve the performance of FPSCs.

The quality of the electron transport layer (ETL) is a crucial factor that affects the efficiency in both rigid and flexible devices[15]. SnO_2 has been considered a promising ETL material due to its high bulk charge mobility(≈250 $cm^2 \cdot V^{-1} \cdot s^{-1}$), wide bandgap, and good energy band alignment with perovskite[16–19]. Low-temperature processed amorphous SnO_2 was first used in planar PSCs in 2015, and achieved an efficiency of over 16%[20]. Since then, a variety of optimizations of SnO_2 to enhance the electron mobility and reduce the surface trap states have been performed, leading to PCEs of more than 25% [21–23]. A variety of SnO_2 deposition techniques have been reported, namely spin-coating[24,25], atomic-layer deposition[26], and magnetron sputtering[27], among which chemical bath deposition[28,29] (CBD) is an attractive option due to its simple fabrication process and coating homogeneity at lower costs. Different from the spin-coating method, the CBD approach is suitable for depositing dense and uniform SnO_2 films without area limits[17,30], which is favorable for the future commercialization of perovskite solar cells[31]. The low-temperature processibility (< 200 °C) makes it compatible with fabrication of flexible perovskite solar cells.

In the CBD process, urea, hydrochloric acid (HCl), water, and tin chloride (II) ($SnCl_2$) are commonly utilized with the addition of thioglycolic acid (TGA) as a complexing agent[21], and an excellent certified PCE of 25.5% has been achieved under optimized CBD conditions[21]. However, uncontrollable nanocrystal growth during CBD process leads to a narrow deposition window for high quality SnO_2 film[21], which in turn results in a unsatisfactory reproducibility. Some methods such as multiple depositions[32] and pre-aging[33] have been reported to alleviate reproducibility problems, however, the new experimental variables make deposition more complicated. Furthermore, the low pH caused by strong acid (HCl) in the chemical bath restricted the application of CBD on the acid-sensitive substrates such as metal foil and flexible transparent conductive oxide (TCO), which are substrates for FPSCs and flexible optoelectronics. Hence, it is highly desirable to develop a controllable SnO_2 deposition process under mild pH to fulfill the requirements for both the deposition of ETL on acid-sensitive flexible substrates for efficient FPSCs and the reproducibility for large-scale applications.

Herein, we report a facile and effective method for SnO_2 CBD by introducing a low-cost tin precursor $SnSO_4$, which not only enables controllable growth and uniform coverage of the high-quality SnO_2 thin film deposition, but also protects the flexible PET/indium tin oxide (ITO) substrate from acid corrosion, facilitating high-performance FPSC fabrication. The FPSCs (Figures 1(a) and 1(b)) were fabricated with the novel CBD-SnO_2 based on $SnSO_4$, achieving a champion PCE of 25.09% (certified 24.90%),

[1]State Key Laboratory of Power System Operation and Control, Department of Electrical Engineering, Tsinghua University, Beijing 100084, China; [2]Center for Excellence in Nanoscience (CAS), Key Laboratory of Nanosystem and Hierarchical Fabrication (CAS), National Center for Nanoscience and Technology, Beijing 100190, China
† These authors contributed equally to this work.
Address correspondence to Chenyi Yi, yicy@tsinghua.edu.cn

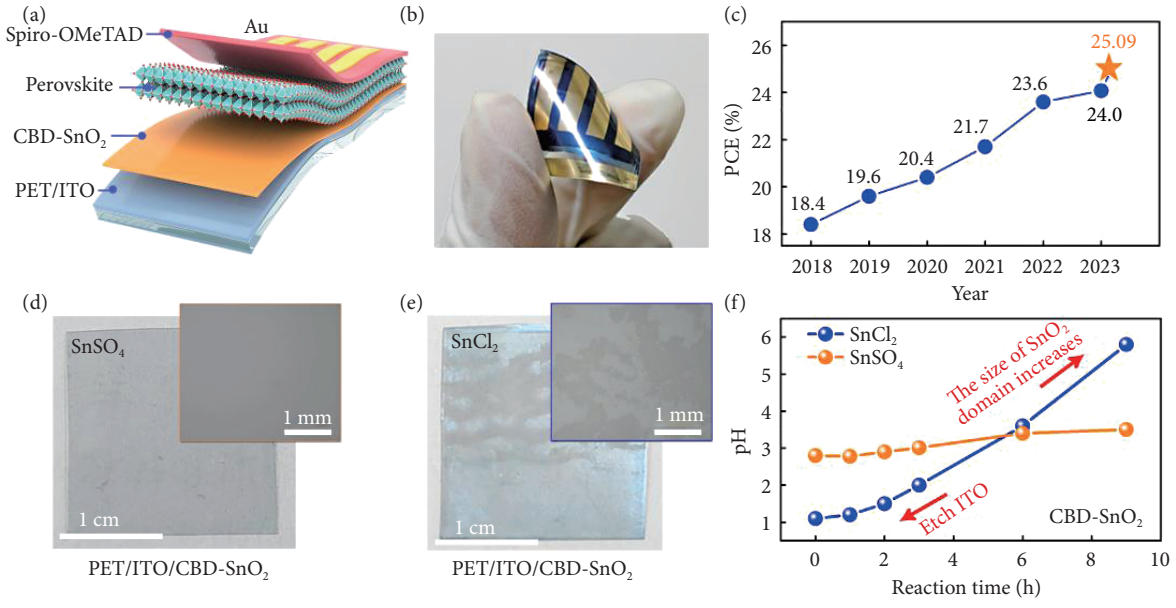

Figure 1 Progress of the highest efficiency of FPSCs and differences in the preparation of SnO_2 films on flexible substrates using $SnCl_2$ and $SnSO_4$. **(a)** Schematic of the structure of the flexible perovskite solar cells. **(b)** Photograph of the FPSCs. **(c)** The progress of reported highest efficiencies for FPSCs in the literature. **(d)** Optical picture and microscope image of the PET/CBD-SnO_2 based on $SnSO_4$. **(e)** Optical picture and microscope image of the PET/CBD-SnO_2 based on $SnCl_2$. **(f)** The variation of pH for two chemical bath solutions with time at 70 °C.

which is the record PCE for FPSCs to date (Figure 1(c)). In addition, $SnSO_4$-based FPSCs exhibited high durability while maintaining over 90% of their initial PCE after 10000 bending cycles. Furthermore, the controllable growth of SnO_2 not only ensures excellent reproducibility of the CBD, but also enables the reutilization of the chemical bath, holding great promise for large-scale applications.

1 Results

1.1 CBD SnO_2 electron transport layer growth

The CBD process shows the ability for facile large area film deposition and high-performance device fabrication, but the commonly used $SnCl_2$-based process cannot be applied directly on the flexible substrates. As vividly shown in Figure 1(e), the PET/ITO substrate suffers serious acid corrosion after 3 h of CBD. The solution pH was monitored during the prolonged process as shown in Figure 1(f). Freshly created CBD solution for typical deposition procedures utilizing $SnCl_2$ has a pH<1.5. Such a low pH value provides a very hostile environment for flexible substrates, which can lead to damaged TCO electrodes with high resistance. Therefore, we employed $SnSO_4$ to substitute $SnCl_2$ as the tin source and removed the strong acid HCl. The $SnSO_4$-based process has a considerably higher and constant pH during the CBD process, which causes no damage to the vulnerable TCO electrode (Figure 1(d)).

During the CBD process, the microstructure of the SnO_2 film is closely related to the reactivity of the transitional species and the crystal particle deposition process[26]. To understand the mechanism of the CBD strategy and its influence on the SnO_2 film morphology, the whole process was analyzed. Basically, the CBD process begins as the tin source ($SnCl_2$ or $SnSO_4$) hydrolyzes and Sn ions in the solution are bonded together to form crystal nuclei. For the $SnCl_2$ case, the crystal nucleus continuously enlarges into nanocrystals, which are suspended in the solution and turn the solution color into milky white (Figure S1 which is in the Electronic Supplementary Material (ESM) in the online version of this paper). As shown in Figure 2(b), after 3 h of CBD, the $SnCl_2$ solution becomes milky, while the $SnSO_4$ solution only changes slightly. The appearance changes of the solution should be related to the light scattering and the size of SnO_2 nanoparticles. Therefore, we determined the nanoparticle size in the CBD solution via transmission electron microscopy (TEM) at different times to understand the growth process. In the $SnSO_4$-based deposition process, the nanoparticles in the solution were all composed of uniform and small particles at different times from 3 h to 9 h (Figure 2(d). In the $SnCl_2$ situation at 3 h, the size of the nanoparticles in the solution varies, and 100 nm nanoparticles start to germinate (Figure 2(c)) which continues to enlarge in size as the growth proceeds to 9 h (Figure S2 in the ESM). The optical transmittance of the solution at 9 h further confirms this result (Figure S3 in the ESM). Dynamic light scattering (DLS) measurements also confirmed the particle size distribution in liquid SnO_2 solution. Clearly, the $SnSO_4$-solution showed smaller particle size, concentrated distribution and smaller time-variation compared to the $SnCl_2$ solution, indicating that the $SnSO_4$ environment could prevent disordered agglomeration of SnO_2 nanoparticles (Figure S4 in the ESM). The different growth behaviors can be attributed to the pH environment and transitional species of the different solutions. Figure 2(a) shows a schematic illustration of SnO_2 films fabricated by chemical bath deposition with two different tin raw materials. In solution with $SnCl_2$, urea, thioglycolic acid, and hydrochloric acid, the pH value increases with longer reaction time due to the decomposition of urea and volatilization of HCl[26]. In the $SnSO_4$ situation, no volatile component is released and the transitional species reactivity is effectively reduced through SO_4^{2-} bonding with Sn^{2+} and forming the assembled complex, which stabilizes the solution pH value and retards the generation of particle agglomeration and oxygen vacancies.

Particle sizes and distribution have great influences on the obtained thin film morphology. To check the applicability of CBD on rough surfaces, we applied fluorine-doped tin oxide (FTO)-

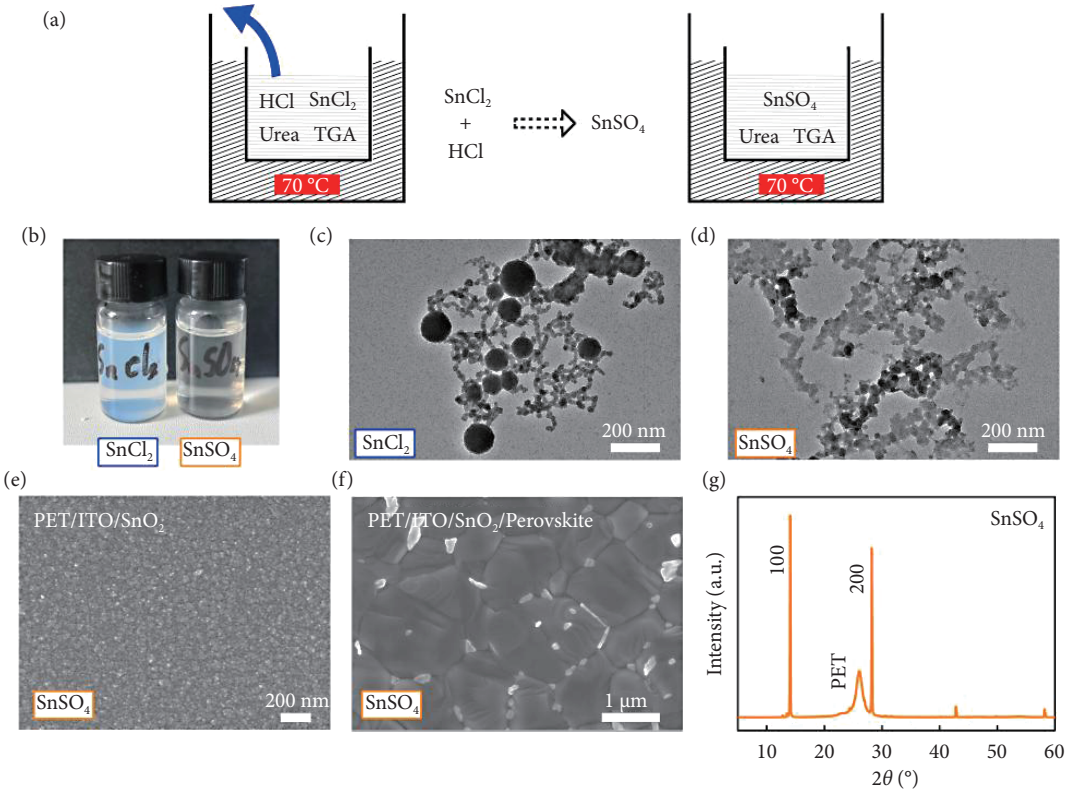

Figure 2 Synthesis and characterization of SnO_2 and perovskite films on flexible substrates. (**a**) Illustration of the two chemical bath processes using different tin sources. (**b**) Photograph of the CBD solution after 3 h at 70 °C. (**c** and **d**) TEM of the particles from the chemical bath of $SnCl_2$ and $SnSO_4$ after 3 h at 70 °C. (**e**) SEM image of SnO_2 film using $SnSO_4$-based method on flexible PET/ITO substrate. (**f**) SEM image of top-view morphology of the perovskite film on $SnSO_4$-ETL on flexible substrate. (**g**) XRD patterns of $FAPbI_3$ deposited on $SnSO_4$-ETL.

covered glass for better observation. The magnified top-right insets highlight the roughness and surface morphology of the film, with the SnO_2 layer clearly sighted on top of a pyramid-shaped FTO domain. The SnO_2 layers are conformal with the underlying FTO layer at 3 h in both situations, except for the $SnCl_2$-substrate, which exhibits a slightly rougher surface (Figures S5 and S6 in the ESM). However, as the reaction time increases to 9 h, the $SnCl_2$-based SnO_2 layer becomes much rougher with oversized SnO_2 clusters coagulating on the FTO surface[21]. Interestingly, the $SnSO_4$-based layer still possesses dense and compact coverage without obvious changes. This means that the $SnSO_4$-based deposition process is more uniform and steadier, which is enabled by the constant pH environment as discussed before. The irregular SnO_2 particle size and morphology resulting from the $SnCl_2$-based method should account for the poor repeatability of CBD in the literature[34,35], while a controllable ETL deposition process enabled by the $SnSO_4$-based method will greatly benefit device fabrication and optimization. As an ETL in PSCs, the optical properties of SnO_2 should also be considered carefully. As shown in Figure S7 in the ESM, both films exhibit a high transmittance in the range of 300–800 nm, which ensures a high current density of planar PSCs.

X-ray photoelectron spectroscopy (XPS) provides the surface elements and chemical bonding configurations of the two kinds of CBD-SnO_2 films. The peak of S emerges at 163 eV, which belongs to the symmetric stretching movement of the S-Sn bond. The new peak appearing at 168 eV in the $SnSO_4$-sample is a symmetric stretching vibration belonging to the S-O bond (Figure S8 in the ESM), in that the SO_4^{2-} moiety can coordinate strongly with Pb^{2+}, which is beneficial for the stability of the devices[36]. When $SnCl_2$ was used as the tin source, a large number of oxygen vacancies were observed (Figure S9 in the ESM), which is harmful to the PSC performance[37]. The oxygen vacancies might be due to the fast growth of SnO_{2-x} and insufficient supply of oxygen dissolved in the solution[26]. In contrast, much fewer oxygen vacancies were found when $SnSO_4$ was used, which is consistent with steady growth rate of SnO_2 film. This is consistent with the improved film quality of the latter, which is beneficial for device performance and stability.

The scanning electron microscopy (SEM) images exhibit a flat surface of SnO_2 films on the flexible substrate by the $SnSO_4$-based method (Figure 2(e)). This is in good agreement with Figure 3(a), which displays the cross-sectional SEM image of the device (PET/ITO/CBD-SnO_2/perovskite/Spiro-OMeTAD/Au), where a compact thin layer of SnO_2 sits between perovskite and ITO. The influences of the flexible SnO_2 layer on perovskite growth were further investigated. SEM images exhibit enlarged perovskite grains with $SnSO_4$ as the material for the top surface (Figure 2(f)), showing grain sizes ranging from 1~2 μm. The perovskite film fabricated on $SnSO_4$-ETL shows a simple $FAPbI_3$ phase as demonstrated in Figure 2(g), with the two strongest diffraction peaks at 14.04° and 28.02° corresponding to the structure of perovskite crystal (1 0 0) and (2 0 0) crystal planes. The wide diffraction peak at approximately 26° is a typical feature of the polymer PET substrate. The UV-vis spectra show that the CBD-SnO_2 based perovskite film exhibits high absorbance with a bandgap of 1.53 eV (Figure S10 in the ESM).

1.2 Device performance and durability

Furthermore, the performances of the FPSCs based on CBD-SnO_2 were investigated by *J-V* characterization, which is not achievable

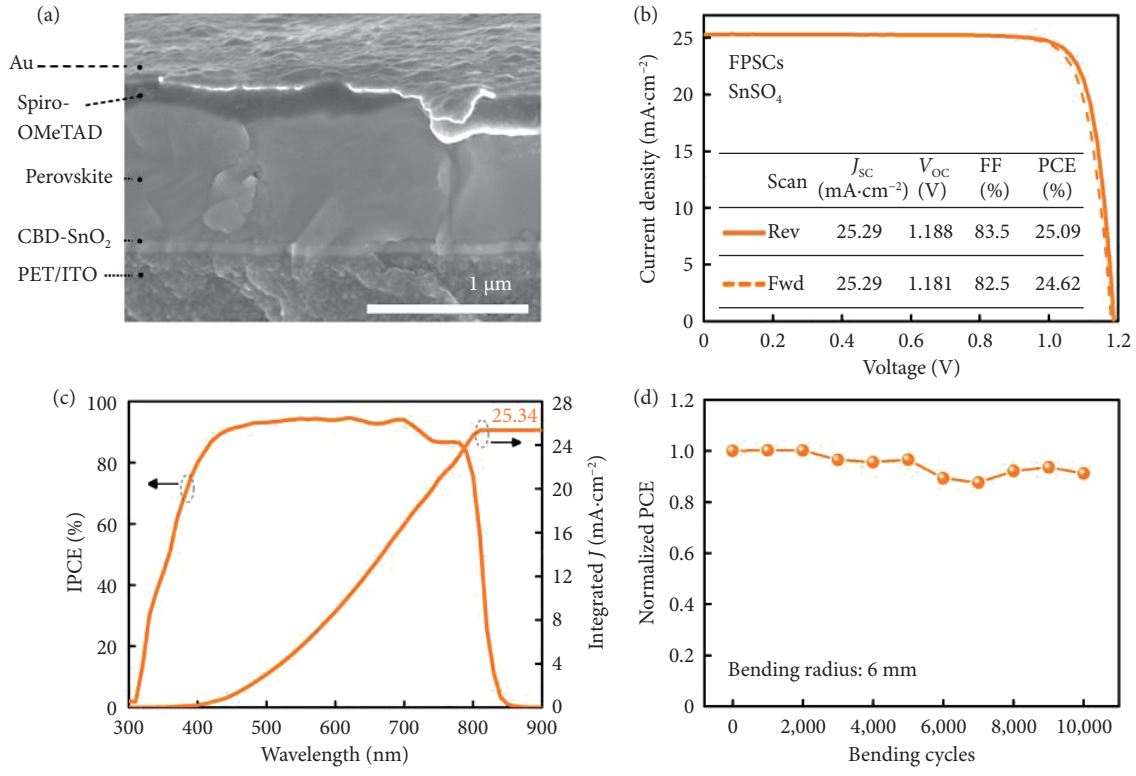

Figure 3 FPSCs device performance. (**a**) Cross-sectional SEM image of the FPSC. (**b**) *J*–*V* curves of the champion FPSCs with $SnSO_4$-ETL. (**c**) IPCE and the integrated J_{SC} of the champion FPSC. (**d**) Bending stability of the FPSC (R = 6 mm, ~30 % RH, ~25 °C).

for the $SnCl_2$ counterpart because of the corrosion problem. The *J*-*V* curves of the champion PSC based on $SnSO_4$-ETL are shown in Figure 3(b). An outstanding efficiency up to 25.09% was achieved, with ashort-circuit current density (J_{SC}) of 25.29 mA/cm^2, a open-circuit voltage (V_{OC}) of 1.188 V, and an fill factor (FF) of 83.5%. We sent one of our FPSCs for certification, and obtained a certificated PCE of 24.90% (reverse scan, 24.67% in forward scan) (Figure S11 in the ESM), which ranks as the highest PCE of FPSCs reported to date (Table S1 in the ESM). The statistics of the photovoltaic metrics for forty FPSCs are summarized in Figure S12 in the ESM, confirming the overall outstanding performance brought by $SnSO_4$-ETL with a uniform distribution and an average PCE of 23.18%. The incident photon-to-current conversion efficiency (IPCE) result is shown in Figure 3(c). An integrated J_{SC} of 25.34 mA/cm^2 indicates a good match with the measured J_{SC}. To evaluate the suitability of the CBD-SnO_2 for fabricating large-area FPSCs, we prepared large-area devices with an aperture area of 1 cm^2, based on the same structure, and achieved a PCE of 21.93% (Figure S13 in the ESM). It demonstrates the scalability of our CBD-SnO_2 protocol. Furthermore, we investigated the mechanical durability of the device by performing continuous bending with a curvature radius of 6 mm. As shown in Figure 3(d), after10000bending cycles, the flexible device based on $SnSO_4$-ETL preserved 90% of the initial efficiency, indicating excellent mechanical stability of our FPSCs. The flexible device based on $SnSO_4$-ETL also demonstrated excellent shelf stability, which maintained 99% of the initial PCE in N_2-filled glove box for 1000 h (Figure S14 in the ESM).

For further comparison, we also checked the performance variation of rigid PSCs with the CBD-SnO_2 optimization strategy. SnO_2-ETL films manufactured using two CBD processes with different tin sources demonstrated similar results in terms of the highest efficiency of rigid devices (FTO substrates were used to prevent the corrosion effects on ITO for the $SnCl_2$-CBD SnO_2). The $SnCl_2$-ETL based device shows a comparable champion PCE of 25.56% (24.48%) with a larger hysteresis (Figure 4(a)). $SnSO_4$-ETL device shows a champion PCE of 25.65% (25.35%), a V_{OC} of 1.190 (1.184) V, a J_{SC} of 25.90 (25.85) mA/cm^2, and an FF of 83.4% (82.6%) under a reverse (forward) voltage scan (Figure 4(b)). The mild growth environment of the $SnSO_4$ precursor with constant pH also benefits the reproducibility and solution reusability of the CBD process. We fabricated a series of PSCs from every 3 h of the total 9 h CBD process using two different precursors (without change solution) to evaluate device performance. All three batches $SnSO_4$-ETL devices exhibited excellent PCEs of more than 24% (Figure 4(c)). We attribute this to the constant solution environment and steady SnO_2 deposition process (Figure S5 in the ESM). Despite the $SnCl_2$-ETL devices showing a comparable average efficiency of approximately 24% in the first 0–3 h batch, the PCE distribution is obviously wider, revealing inferior uniformity. Furthermore, we observed a sharp drop in device performance for the latter two batches (Figure 4(c)). The device performance agreed perfectly with the different morphologies of the two kinds of ETLs (Figure 2(c), Figures S2 and S5 in the ESM). The reusability of raw materials is beneficial for significantly reducing the manufacturing costs of CBD-SnO_2. In addition, the relatively more concentrated distribution of device performance is beneficial for improving the yield of device preparation. Moreover, the CBD method based on $SnSO_4$ exhibits good controllability and reproducibility, making it a promising candidate for large-scale production in the future.

Apart from the improved reproducibility, we found that the $SnSO_4$-ETL devices primarily showed improved thermal stability at 85 °C in a nitrogen environment. The $SnSO_4$-ETL device maintained 85% of its initial performance (Figure 4(d)), after 500 h of continuous heating. In comparison, the $SnCl_2$-ETL device dropped quickly to 23% of its initial PCE after 200 h of continuous

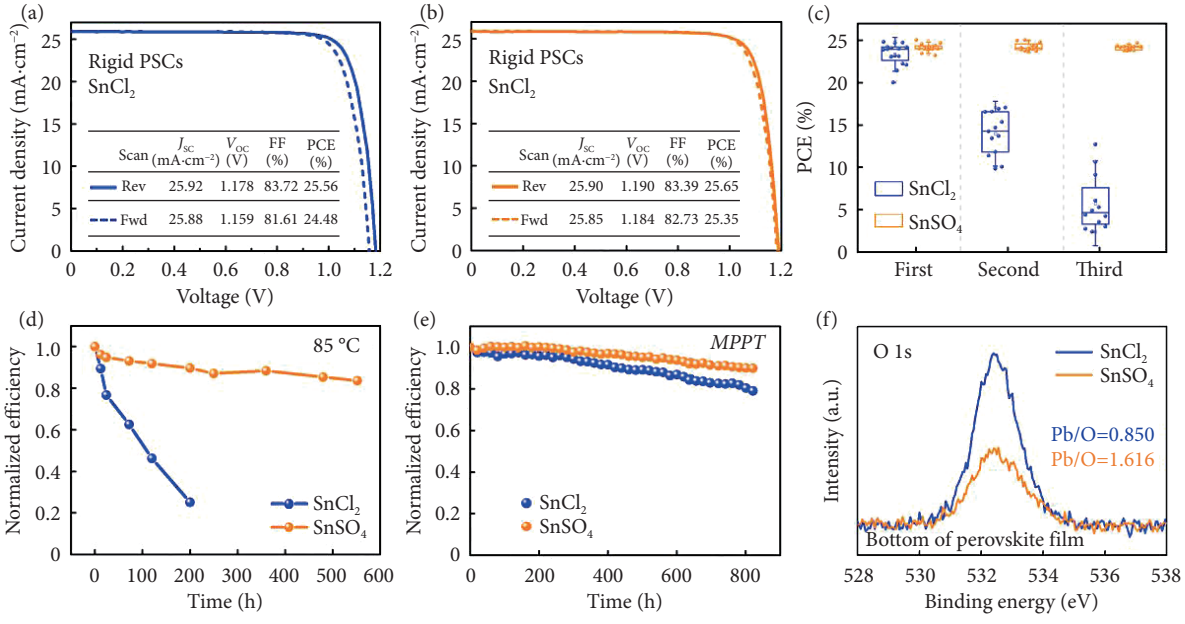

Figure 4 Performance of rigid PSCs with different ETLs. (**a**, **b**) *J*–*V* curves and photovoltaic metrics of the champion rigid PSCs based on $SnCl_2$-ETL (a) and $SnSO_4$-ETL (b). (**c**) PCE statistics for the PSCs with SnO_2 ETL deposited in the same $SnCl_2$ and $SnSO_4$ chemical bath solution at different times (First 0–3 h; Second 3–6 h; Third 6–9 h). (**d**) Thermal stability (85 °C) of rigid PSCs based on $SnCl_2$ and $SnSO_4$-ETL. (**e**) Light-soaking stability of devices measured under maximum power point (*MPPT*). The devices were tested with 100 mW/cm² illumination under 25 °C under N_2. (**f**) O 1s spectra results obtained on the exposed buried interface of the aged perovskite films based on $SnCl_2$ and $SnSO_4$-ETL.

heating. In addition, $SnSO_4$-ETL devices also exhibited better light stability at maximum power-point tracking (*MPPT*), under 100 mW/cm² illumination in N_2. The PCE of the $SnCl_2$-ETL device gradually decayed to 80% after aging for 800 h. In comparison, $SnSO_4$-based devices maintained 90% of their initial PCE under the same conditions (Figure 4(e)). To understand this result, we exposed the buried interface of perovskite films and performed XPS measurements to carefully probe the interaction between the SnO_2 layers and the perovskite active layer (Figure 4(f)). The perovskite thin film prepared on the $SnCl_2$-ETL substrate has more oxygen absorption species at the bottom interface, implying a more seriously decomposed interface. We also directly subjected the perovskite films on these two different ETLs to a high temperature treatment of 150 °C to further assess their thermal stability. After being heated for 1 hour, the perovskite film on $SnCl_2$-ETL showed a prominent peak of PbI_2 while that on $SnSO_4$-ETL only decomposed partly and maintained the black feature (Figure S15 in the ESM). We speculate that the enhanced thermal stability to the reduced oxygen vacancy on the ETL and the strong interfacial interaction between the SO_4^{2-} moiety of $SnSO_4$-ETL and Pb^{2+}[36].

2 Conclusions

In summary, an effective CBD method was proposed for preparing SnO_2 ETLs by utilizing $SnSO_4$ as the tin source. Compared to the $SnCl_2$ counterpart with volatile HCl addition, the nonvolatile nature of the $SnSO_4$ precursor provided a mild and controllable environment for thin film deposition, which ensured uniform SnO_2 nanoparticle growth and a dense film with full coverage. The constant pH of the chemical bath solution without strong acid enabled quality SnO_2 ETL deposited on the flexible substrates without corrosion and the reusability of the CBD solution. As a result, a record PCE of 25.09% (certified 24.90%) was achieved for FPSCs with excellent mechanical durability, retaining 90% of the initial PCE after 10000 bending cycles (bending radius: 6 mm). The excellent performance, wide applicability and reusability of this novel CDB SnO_2 holds great promise for large-scale application of PSCs.

Acknowledgements

This work is financially supported by the National Key Research and Development Program of China (2022YFB3803304), National Natural Science Foundation of China (U23B20153, U23A20138), Tsinghua University Initiative Scientific Research Program (20221080065, 20223080044), Independent Innovative Research Program (ZK20230101), Department of Electrical Engineering, Tsinghua University, State Key Laboratory of Power System and Generation Equipment (Nos. SKLD21Z03 and SKLD20M03); China Postdoctoral Science Foundation (2023M741888), The Chinese Thousand Talents Program for Young Professionals; State Grid Corporation of China, National Bio Energy Co. Ltd., grant no. 52789922000D.

Author Contributions

N. R., L. T., and M. L. contributed equally to this work. C. Y. conceived the idea and directed the project. N. R., and L. T. performed the experiments. N. R., L. T., and M. L. prepared the draft. All the authors participated in the discussion of the results and revision of the manuscript.

Article history

Received: 19 February 2024; Revised: 5 March 2024; Accepted: 15 March 2024

Additional information

Electronic Supplementary Material The online version contains supplementary material available at https://doi.org/10.23919/IEN.2024.0001.

Declaration of competing interest

A patent has been filed based on this research.

References

[1] Xu, R., Pan, F., Chen, J., Li, J., Yang, Y., Sun, Y., Zhu, X., Li, P., Cao, X., Xi, J., et al. (2024). Optimizing the buried interface in flexible perovskite solar cells to achieve over 24% efficiency and long-term stability. *Advanced Materials*, 36: 2308039.

[2] Yang, L., Feng, J., Liu, Z., Duan, Y., Zhan, S., Yang, S., He, K., Li, Y., Zhou, Y., Yuan, N., et al. (2022). Record-efficiency flexible perovskite solar cells enabled by multifunctional organic ions interface passivation. *Advanced Materials*, 34: 2201681.

[3] You, S., Zeng, H., Ku, Z., Wang, X., Wang, Z., Rong, Y., Zhao, Y., Zheng, X., Luo, L., Li, L., et al. (2020). Multifunctional polymer-regulated SnO_2 nanocrystals enhance interface contact for efficient and stable planar perovskite solar cells. *Advanced Materials*, 32: 2003990.

[4] Ru, P., Bi, E., Zhang, Y., Wang, Y., Kong, W., Sha, Y., Tang, W., Zhang, P., Wu, Y., Chen, W., et al. (2020). High electron affinity enables fast hole extraction for efficient flexible inverted perovskite solar cells. *Advanced Energy Materials*, 10: 1903487.

[5] Meng, X., Cai, Z., Zhang, Y., Hu, X., Xing, Z., Huang, Z., Huang, Z., Cui, Y., Hu, T., Su, M., et al. (2020). Bio-inspired vertebral design for scalable and flexible perovskite solar cells. *Nature Communications*, 11: 3016.

[6] Li, M., Zhou, J., Tan, L., Li, H., Liu, Y., Jiang, C., Ye, Y., Ding, L., Tress, W., Yi, C. (2022). Multifunctional succinate additive for flexible perovskite solar cells with more than 23% power-conversion efficiency. *The Innovation*, 3: 100310.

[7] Li, L., Wang, Y., Wang, X., Lin, R., Luo, X., Liu, Z., Zhou, K., Xiong, S., Bao, Q., Chen, G., et al. (2022). Flexible all-perovskite tandem solar cells approaching 25% efficiency with molecule-bridged hole-selective contact. *Nature Energy*, 7: 708–717.

[8] Lei, Y., Chen, Y., Zhang, R., Li, Y., Yan, Q., Lee, S., Yu, Y., Tsai, H., Choi, W., Wang, K., et al. (2020). A fabrication process for flexible single-crystal perovskite devices. *Nature*, 583: 790–795.

[9] Chung, J., Shin, S. S., Hwang, K., Kim, G., Kim, K. W., Lee, D. S., Kim, W., Ma, B. S., Kim, Y. K., Kim, T. S., et al. (2020). Record-efficiency flexible perovskite solar cell and module enabled by a porous-planar structure as an electron transport layer. *Energy & Environmental Science*, 13: 4854–4861.

[10] Kumar, M. H., Yantara, N., Dharani, S., Graetzel, M., Mhaisalkar, S., Boix, P. P., Mathews, N. (2013). Flexible, low-temperature, solution processed ZnO-based perovskite solid state solar cells. *Chemical Communications*, 49: 11089–11091.

[11] Wu, Y., Xu, G., Xi, J., Shen, Y., Wu, X., Tang, X., Ding, J., Yang, H., Cheng, Q., Chen, Z., et al. (2023). *In situ* crosslinking-assisted perovskite grain growth for mechanically robust flexible perovskite solar cells with 23.4% efficiency. *Joule*, 7: 398–415.

[12] Xie, L., Du, S., Li, J., Liu, C., Pu, Z., Tong, X., Liu, J., Wang, Y., Meng, Y., Yang, M., et al. (2023). Molecular dipole engineering-assisted strain release for mechanically robust flexible perovskite solar cells. *Energy & Environmental Science*, 16: 5423–5433.

[13] Park, J., Kim, J., Yun, H. S., Paik, M. J., Noh, E., Mun, H. J., Kim, M. G., Shin, T. J., Seok, S. I. (2023). Controlled growth of perovskite layers with volatile alkylammonium chlorides. *Nature*, 616: 724–730.

[14] Xu, W., Chen, B., Zhang, Z., Liu, Y., Xian, Y., Wang, X., Shi, Z., Gu, H., Fei, C., Li, N., et al. (2024). Multifunctional entinostat enhances the mechanical robustness and efficiency of flexible perovskite solar cells and minimodules. *Nature Photonics*, https://doi.org/10.1038/s41566-023-01373-z.

[15] Elseman, A. M., Xu, C., Yao, Y., Elisabeth, M., Niu, L., Malavasi, L., Song, Q. L. (2020). Electron transport materials: Evolution and case study for high-efficiency perovskite solar cells. *Solar RRL*, 4: 2000136.

[16] Wu, P., Wang, S., Li, X., Zhang, F. (2021). Advances in SnO_2-based perovskite solar cells: From preparation to photovoltaic applications. *Journal of Materials Chemistry A*, 9: 19554–19588.

[17] Park, S. Y., Zhu, K. (2022). Advances in SnO_2 for efficient and stable n–i–p perovskite solar cells. *Advanced Materials*, 34: 2110438.

[18] Uddin, A., Yi, H. (2022). Progress and challenges of SnO_2 electron transport layer for perovskite solar cells: A critical review. *Solar RRL*, 6: 2100983.

[19] Jiang, Q., Zhang, X., You, J. (2018). SnO_2: A wonderful electron transport layer for perovskite solar cells. *Small*, 14: 1801154.

[20] Ke, W., Fang, G., Liu, Q., Xiong, L., Qin, P., Tao, H., Wang, J., Lei, H., Li, B., Wan, J., et al. (2015). Low-temperature solution-processed tin oxide as an alternative electron transporting layer for efficient perovskite solar cells. *Journal of the American Chemical Society*, 137: 6730–6733.

[21] Yoo, J. J., Seo, G., Chua, M. R., Park, T. G., Lu, Y., Rotermund, F., Kim, Y. K., Moon, C. S., Jeon, N. J., Correa-Baena, J. P., et al. (2021). Efficient perovskite solar cells via improved carrier management. *Nature*, 590: 587–593.

[22] Min, H., Lee, D. Y., Kim, J., Kim, G., Lee, K. S., Kim, J., Paik, M. J., Kim, Y. K., Kim, K. S., Kim, M. G., et al. (2021). Perovskite solar cells with atomically coherent interlayers on SnO_2 electrodes. *Nature*, 598: 444–450.

[23] Kim, M., Jeong, J., Lu, H., Lee, T. K., Eickemeyer, F. T., Liu, Y., Choi, I. W., Choi, S. J., Jo, Y., Kim, H. B., et al. (2022). Conformal quantum dot–SnO_2 layers as electron transporters for efficient perovskite solar cells. *Science*, 375: 302–306.

[24] Zhao, Y., Ma, F., Qu, Z., Yu, S., Shen, T., Deng, H. X., Chu, X., Peng, X., Yuan, Y., Zhang, X., et al. (2022). Inactive $(PbI_2)_2RbCl$ stabilizes perovskite films for efficient solar cells. *Science*, 377: 531–534.

[25] Halvani Anaraki, E., Kermanpur, A., Mayer, M. T., Steier, L., Ahmed, T., Turren-Cruz, S. H., Seo, J., Luo, J., Zakeeruddin, S. M., Tress, W. R., et al. (2018). Low-temperature Nb-doped SnO_2 electron-selective contact yields over 20% efficiency in planar perovskite solar cells. *ACS Energy Letters*, 3: 773–778.

[26] Lee, S. U., Park, H., Shin, H., Park, N. G. (2023). Atomic layer deposition of SnO_2 using hydrogen peroxide improves the efficiency and stability of perovskite solar cells. *Nanoscale*, 15: 5044–5052.

[27] Peng, Z., Zuo, Z., Qi, Q., Hou, S., Fu, Y., Zou, D. (2023). Perovskite solar cells with all functional layers deposited by magnetron sputtering. *ACS Applied Energy Materials*, 6: 7556–7562.

[28] Gao, L., He, Z., Zeng, K., Liu, A., Jiang, F., Ma, T. (2023). Ultralow-temperature SnO_2 electron transport layers fabricated by intermediate-controlled chemical bath deposition for highly efficient perovskite solar cells. *ChemSusChem*, 16: 2300765.

[29] Tay, D. J. J., Febriansyah, B., Salim, T., Wong, Z. S., Dewi, H. A., Koh, T. M., Mathews, N. (2023). Enabling a rapid SnO_2 chemical bath deposition process for perovskite solar cells. *Sustainable Energy & Fuels*, 7: 1302–1310.

[30] Wu, Z., Su, J., Chai, N., Cheng, S., Wang, X., Zhang, Z., Liu, X., Zhong, H., Yang, J., Wang, Z., et al. (2023). Periodic acid modification of chemical-bath deposited SnO_2 electron transport layers for perovskite solar cells and mini modules. *Advanced Science*, 10: 2300010.

[31] Pawar, S. M., Pawar, B. S., Kim, J. H., Joo, O. S., Lokhande, C. D. (2011). Recent status of chemical bath deposited metal chalcogenide and metal oxide thin films. *Current Applied Physics*, 11: 117–161.

[32] Zimmermann, I., Provost, M., Mejaouri, S., Al Atem, M., Blaizot, A., Duchatelet, A., Collin, S., Rousset, J. (2022). Industrially compatible fabrication process of perovskite-based mini-modules coupling sequential slot-die coating and chemical bath deposition. *ACS Applied Materials & Interfaces*, 14: 11636–11644.

[33] Zhao, Q., Liu, D., Li, Z., Zhang, B., Sun, X., Shao, Z., Chen, C., Wang, X., Hao, L., Wang, X., et al. (2022). Chemical bath deposition

of mesoporous SnO_2 to improve interface adhesion and device operational stability. *Chemical Engineering Journal*, 443: 136308.

[34] Zhang, J., Bai, C., Dong, Y., Shen, W., Zhang, Q., Huang, F., Cheng, Y. B., Zhong, J. (2021). Batch chemical bath deposition of large-area SnO_2 film with mercaptosuccinic acid decoration for homogenized and efficient perovskite solar cells. *Chemical Engineering Journal*, 425: 131444.

[35] Ko, Y., Kim, Y., Lee, C., Kim, T., Kim, S., Yun, Y. J., Gwon, H. J., Lee, N. H., Jun, Y. (2020). Self-aggregation-controlled rapid chemical bath deposition of SnO_2 layers and stable dark depolarization process for highly efficient planar perovskite solar cells. *ChemSusChem*, 13: 4051–4063.

[36] Yang, S., Chen, S., Mosconi, E., Fang, Y., Xiao, X., Wang, C., Zhou, Y., Yu, Z., Zhao, J., Gao, Y., et al. (2019). Stabilizing halide perovskite surfaces for solar cell operation with wide-bandgap lead oxysalts. *Science*, 365: 473–478.

[37] Lee, J. H., Lee, S., Kim, T., Ahn, H., Jang, G. Y., Kim, K. H., Cho, Y. J., Zhang, K., Park, J. S., Park, J. H. (2023). Interfacial α-$FAPbI_3$ phase stabilization by reducing oxygen vacancies in SnO_{2-x}. *Joule*, 7: 380–397.